Coupled Systems Mechanics, *Vol. 9, No. 1 (2020) 29-46*
DOI: https://doi.org/10.12989/csm.2020.9.1.029

Buckling analysis of complex structures with refined model built of frame and shell finite elements

Emina Hajdo*[1], Adnan Ibrahimbegovic[2a] and Samir Dolarevic[1b]

[1]*Faculty of Civil Engineering, University of Sarajevo, Sarajevo, Bosnia and Herzegovina*
[2]*Laboratoire Roberval, Université de Technologie de Compiègne / Sorbonne Universités, France*

(Received July 9, 2019, Revised November 1, 2019, Accepted January 13, 2020)

Abstract. In this paper we deal with stability problems of any complex structure that can be modeled by beam and shell finite elements. We use for illustration the steel plate girders, which are used in bridge construction, and in industrial halls or building construction. Long spans, slender cross sections exposed to heavy loads, are all critical design points engineers must take into account. Knowing the critical load that will cause lateral torsional buckling of the girder, or load that can lead to web buckling, as an important scenario to consider in a design process. Many of such problem, including lateral torsional buckling with influence of lateral supports and their spacing on critical load can be solved by the proposed method. An illustrative study of web buckling also includes effects of position and spacing of transverse and longitudinal web stiffeners, where stiffeners can be modelled optionally using shell or frame elements.

Keywords: stability; steel plate girder; web buckling; lateral torsional buckling; critical load; shell model

1. Introduction

Thin steel plates are widely used in everyday engineering practice (structural engineering, shipbuilding, aircraft industry). Structural engineers have been facing a challenge imposed by architectural demands for "elegant" and slender structures. In particular, the design of slender structures has to include buckling analysis of trusses (Ibrahimbegovic *et al*. 2013), columns (Ngo *et al*. 2014), plates and more complex structures yet to be solved for the most general case. At present, the engineers mostly use frame elements in computational models when analysing behavior of the I-shaped steel sections. It is important to emphasize that such a model can take into account only global stability of the beam. This can be done using for example geometrically non-linear beam finite elements (e.g., Ibrahimbegovic and Frey 1993, Ibrahimbegovic 1995, Ibrahimbegovic *et al*. 1996, Imamovic *et al*. 2017, Imamovic *et al*. 2018). Using shell elements in modelling parts of I-shaped steel section (flanges and web), it is possible to investigate the local buckling of each particular section element. Given that welded plate girders are widely spread in construction of bridges and buildings, and that they can have a very complex form due to stiffeners, the present situation should be imposed. Namely, the main advantages of lightweight structure, long spans,

*Corresponding author, Ph.D., E-mail: emina.hajdo@gmail.com
[a]Professor, E-mail: adnan.ibrahimbegovic@utc.fr
[b]Professor, E-mail: samir.dolarevic@gf.unsa.ba

http://www.techno-press.org/?journal=csm&subpage=8 ISSN: 2234-2184 (Print), 2234-2192 (Online)

different shapes and dimensions of cross section are at present diminish with the lack of predictive models for not only global but also local instability. We will illustrate the proposed approach for different shapes, such as rectangular, cylindrical, U-shaped and I-shaped complex structures. We will show its efficiency and accuracy for large cross-section slenderness, defined by d/t_w ratio, where d is cross section height and t_w is web thickness.

We will improve upon the currently valid recommendation of the design code (EC3), which recommends values of web slenderness ratio (h_w/t_w, where h_w is web height) to avoid web buckling problems. If the limit value h_w/t_w is exceeded, the plastic shear resistance $V_{pl,Rd}$ can never be reached, and it is necessary to calculate new reduced value $V_{b,Rd}$ (EC 3 2006).

Nowadays steelmaking process can secure the high-strength of steel members. Their use can significantly reduce the self-weight of the structural members, but it is necessary to properly secure the stiffness of such a members to avoid loss of stability. In some cases, when beams are not supported with sufficient number of lateral restraints, the lateral torsional buckling may occur. Many recent works deal with lateral torsional buckling of steel girders (e.g., Kala 2015, Bredford and Liu 2016, Kala and Valeš 2017, Mudenda and Zingoni 2018, Ozbasaran and Yilmaz 2018, Bas 2019, Gonçalves 2019, Sahraei and Mohareb 2019). Making the web thickness too small can cause different forms of web instability such as shear or compression buckling of the web (e.g., Saliba and Gardner 2013, Serror *et al.* 2016, Ellobodya 2017).

The model presented here can easily give us the critical load value, and allow us to optimize lateral supports spacing, as well as stiffeners spacing and geometry.

The main novelty of the proposed model is in the computational procedure for computing the critical load due to buckling, or linear instability (e.g., Ibrahimbegovic 2009). The model can use any of four nodes shell elements accounting for drilling rotations (Ibrahimbegovic *et al*. 1990, Ibrahimbegovic 1994, Ibrahimbegovic and Frey 1994a, Ibrahimbegovic and Frey 1994b, Ibrahimbegovic and Frey 1995). The element is capable of modelling the behavior of structure subjected to mechanical loading, and of taking into account geometric nonlinearities due to buckling problems. We considered small pre-buckling displacements, which leads to linear kinematics and nonlinear equilibrium equations (Ibrahimbegovic *et al*. 2013). Critical value of load parameter is obtained by solving the general eigenvalue problem (Ibrahimbegovic and Wilson 1990, Ibrahimbegovic *et al*. 1990a, Bathe 1996).

The outline of our paper is as follows. In Section 2, we present theoretical formulation of flat shell for buckling analysis. Its discrete approximation is constructed by FEM as shown in Section 3. In Section 4 we give several illustration examples, and in Section 5 we state conclusions.

2. Geometric instability problems of plates and shells

Loads acting in plane of the flat shell may result in loss of its stability, by buckling. An analytical solution for the buckling of the rectangular plates can be obtained by using energy methods or by solving the differential plate equation (Timoshenko and Gere 1962). For the rectangular plate simply supported at all four edges, and loaded with in-plane constant pressure N_x (see Fig. 1), the critical load is given as

$$N_x = \frac{\pi^2 E t^3}{12(1-\nu^2)}\left(\frac{m}{a}+\frac{n^2 a}{m b^2}\right)^2 \tag{1}$$

where m and n represent the number of half sine waves in two directions of the plate, E is Young's

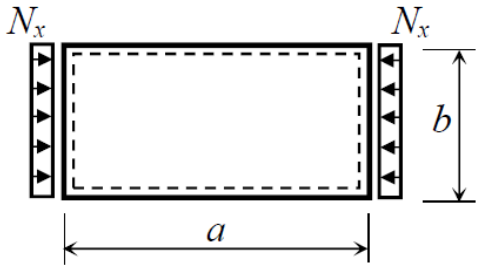

Fig. 1 Simply supported beam with compression load in its plane

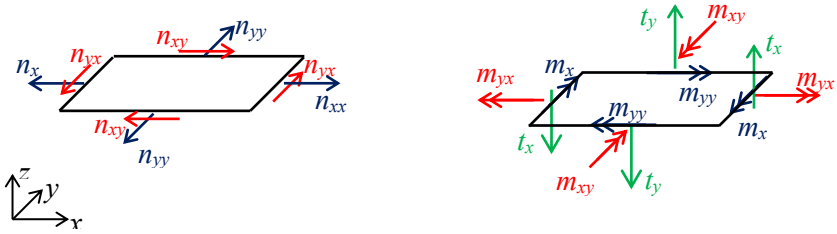

Fig. 2 Stress resultants in shell (membrane and plate)

modulus, v is Poisson's ratio, a and b are plate spans, and t is plate thickness. The critical force $N_{x,cr}$ is the smallest value of the N_x. Namely, when n=1, Eq. (1) will give the critical value of N_x

$$N_{x,cr} = \frac{\pi^2 E t^3}{12(1-v^2)b^2} k_\sigma; \quad k_\sigma = \left[m\frac{b}{a} + \frac{1}{m}\frac{a}{b}\right]^2 \tag{2}$$

Since Eq. (2) depends on m, and plate span ratio, the critical force $N_{x,cr}$ can be calculated by minimizing with respect to m, leading to the minimum value of coefficient k_σ. More details on this analytical solution can be found in Timoshenko and Gere (1962), Chajes (1974) etc.

Needless to say, any such analytical solution is much more difficult, if not impossible, to obtain for more complex case. Nevertheless, the simple case of rectangular plate buckling serves very well for validation of the model proposed herein. Namely, linear buckling analysis of plated structures will be performed by using quadrilateral four node flat shell element. The flat shell finite element can easily be derived by superposition of a plate finite element and a membrane finite element (Fig. 2). Here, we use the Reissner-Mindlin plate theory to define plate element, and the membrane with drilling rotation (Ibrahimbegovic *et al*. 1990, Ibrahimbegovic 1994, Ibrahimbegovic and Frey 1994a, Ibrahimbegovic and Frey 1994b, Ibrahimbegovic and Frey 1995). In the proposed formulation, however, we will also include the simplified nonlinear strain-displacement relations. The resulting shell element has six degrees of freedom per node, three translations and three rotations. The complete displacement vector is given in Eq. (3). Detailed membrane and plate theory analysis can be found in standard reference books (e.g., Timoshenko and Woinowsky-Krieger 1959, Ventsel and Krauthammer 2001).

$$\{u\} = \{u_{0x} \;\; u_{0y} \;\; u_{0z} \;\; \theta_y \;\; \theta_x \;\; \theta_z\}^T \tag{3}$$

$$\varepsilon_{mx} = \frac{\partial u_{0x}}{\partial x} \qquad\qquad \kappa_y = \frac{\partial \theta_y}{\partial x}$$

$$\begin{aligned} \varepsilon_{my} &= \frac{\partial u_{0y}}{\partial y} & \kappa_x &= \frac{\partial \theta_x}{\partial y} \\ \gamma_{mxy} &= \frac{\partial u_{0x}}{\partial y} + \frac{\partial u_{0y}}{\partial x} & \kappa_{xy} &= \frac{1}{2}\left(\frac{\partial \theta_y}{\partial y} + \frac{\partial \theta_x}{\partial x}\right) \end{aligned} \tag{4}$$

If we denote linear theory deformation measures for membrane and plate part as given in Eq. (4), we can further rewrite the membrane deformations for nonlinear case by introducing the von Karman deformation measure. The latter is valid for the case of small deformations and moderate rotations, leading to expression defined in Eq. (5).

$$\{\varepsilon_m\} = \{\varepsilon_{m1}\} + \{\varepsilon_{m2}\} = \begin{Bmatrix} \frac{\partial u_{0x}}{\partial x} \\ \frac{\partial u_{0y}}{\partial y} \\ \frac{\partial u_{0x}}{\partial y} + \frac{\partial u_{0y}}{\partial x} \end{Bmatrix} + \begin{Bmatrix} \frac{1}{2}\left(\frac{\partial u_{0z}}{\partial x}\right)^2 \\ \frac{1}{2}\left(\frac{\partial u_{0z}}{\partial y}\right)^2 \\ \frac{\partial u_{0z}}{\partial x}\frac{\partial u_{0z}}{\partial y} \end{Bmatrix} \tag{5}$$

The corresponding stress resultants for the plate are further decomposed into the bending and shear, which can be written

$$\begin{Bmatrix} \{m\} \\ \{t\} \end{Bmatrix} = \begin{bmatrix} [D_\kappa] & 0 \\ 0 & [D_\gamma] \end{bmatrix} \begin{Bmatrix} \{\kappa\} \\ \{\gamma\} \end{Bmatrix} \tag{6}$$

The component form of force and deformation vectors are defined as

$$\{m\} = \begin{Bmatrix} m_{xx} \\ m_{yy} \\ m_{xy} \end{Bmatrix};\ \{t\} = \begin{Bmatrix} t_{xz} \\ t_{yz} \end{Bmatrix};\ \{\kappa\} = \begin{Bmatrix} \kappa_{yy} \\ \kappa_{xx} \\ 2\kappa_{xy} \end{Bmatrix};\ \{\gamma\} = \begin{Bmatrix} \gamma_{xz} \\ \gamma_{yz} \end{Bmatrix} \tag{7}$$

The corresponding constitutive matrices $\mathbf{D}_\kappa$ and $\mathbf{D}_\gamma$ are written as

$$[D_\kappa] = \frac{E \cdot t^3}{12(1-v^2)} \begin{bmatrix} 1 & v & 0 \\ v & 1 & 0 \\ 0 & 0 & \frac{1-v}{2} \end{bmatrix};\ [D_\gamma] = \frac{E \cdot t}{2(1+v)} \begin{bmatrix} 1 & 0 \\ 0 & 1 \end{bmatrix} \tag{8}$$

Furthermore, the membrane resultants are also defined through constitutive equation

$$\{n\} = [D_m]\{\varepsilon_m\};\ \{n\} = \begin{Bmatrix} n_{xx} \\ n_{yy} \\ n_{xy} \end{Bmatrix};\ [D_m] = \frac{E \cdot t}{1-v^2} \begin{bmatrix} 1 & v & 0 \\ v & 1 & 0 \\ 0 & 0 & \frac{1-v}{2} \end{bmatrix} \tag{9}$$

where the membrane strain $\boldsymbol{\varepsilon}_\mathbf{m}$ is defined in Eq. (5). Next, we denote the virtual displacement of shell Eq. (10). The resulting virtual deformations of the plate part $\boldsymbol{\delta\kappa}$ and $\boldsymbol{\delta\gamma}$ are as follows

$$\begin{aligned} \{\omega\} &= \{\omega_x\ \ \omega_y\ \ \omega_z\ \ \delta\theta_y\ \ \delta\theta_x\ \ \delta\theta_y\}^T \\ \{\delta\kappa\} &= \begin{Bmatrix} \delta\kappa_{yy} \\ \delta\kappa_{xx} \\ 2\delta\kappa_{xy} \end{Bmatrix};\ \{\delta\gamma\} = \begin{Bmatrix} \delta\gamma_{xz} \\ \delta\gamma_{yz} \end{Bmatrix} \end{aligned} \tag{10}$$

By superposing the real and virtual displacements we can define the perturbed configuration

$$\begin{Bmatrix} u_{x\alpha} \\ u_{y\alpha} \\ u_{z\alpha} \end{Bmatrix} = \begin{Bmatrix} u_x \\ u_y \\ u_z \end{Bmatrix} + \begin{Bmatrix} \alpha \cdot \omega_x \\ \alpha \cdot \omega_y \\ \alpha \cdot \omega_z \end{Bmatrix} \tag{11}$$

These virtual von Karman deformations can be obtained by using the directional or Gâteaux derivative (e.g., see Ibrahimbegovic 2009) in the direction of the virtual displacements, which leads to

$$\begin{Bmatrix} \delta\varepsilon_{mx} \\ \delta\varepsilon_{my} \\ \delta\gamma_{mxy} \end{Bmatrix} = \begin{Bmatrix} \delta\varepsilon_{mx1} \\ \delta\varepsilon_{my1} \\ \delta\gamma_{mxy1} \end{Bmatrix} + \begin{Bmatrix} \delta\varepsilon_{mx2} \\ \delta\varepsilon_{my2} \\ \delta\gamma_{mxy2} \end{Bmatrix} = \begin{Bmatrix} \frac{\partial\omega_x}{\partial x} \\ \frac{\partial\omega_y}{\partial y} \\ \frac{\partial\omega_x}{\partial y} + \frac{\partial\omega_y}{\partial x} \end{Bmatrix} + \begin{Bmatrix} \frac{\partial\omega_z}{\partial x}\frac{\partial u_z}{\partial x} \\ \frac{\partial\omega_z}{\partial y}\frac{\partial u_z}{\partial y} \\ \frac{\partial\omega_z}{\partial y}\frac{\partial u_z}{\partial x} + \frac{\partial\omega_z}{\partial x}\frac{\partial u_z}{\partial y} \end{Bmatrix} \tag{12}$$

The virtual deformation given in Eq. (12) can also be written in vector notation, which we will denote

$$\{\partial\varepsilon_m\} = \{\partial\varepsilon_{m1}\} + \{\partial\varepsilon_{m2}\} \tag{13}$$

The virtual work of internal forces can be decomposed into virtual work of membrane forces and virtual work of plate forces

$$\begin{aligned} V_{int} &= \int_\Omega \begin{Bmatrix} \delta\varepsilon_{mx} \\ \delta\varepsilon_{my} \\ \delta\gamma_{mxy} \end{Bmatrix}^T \begin{Bmatrix} n_{xx} \\ n_{yy} \\ n_{xy} \end{Bmatrix} d\Omega + \int_\Omega \begin{Bmatrix} \delta\kappa_{yy} \\ \delta\kappa_{xx} \\ 2\delta\kappa_{xy} \\ \delta\gamma_{xz} \\ \delta\gamma_{yz} \end{Bmatrix}^T \begin{Bmatrix} m_{xx} \\ m_{yy} \\ m_{xy} \\ t_{xz} \\ t_{yz} \end{Bmatrix} d\Omega \\ &= \int_\Omega \{\delta\varepsilon_m\}^T \{n\} d\Omega + \int_\Omega \begin{Bmatrix} \{\delta\kappa\} \\ \{\delta\gamma\} \end{Bmatrix}^T \begin{Bmatrix} \{m\} \\ \{t\} \end{Bmatrix} d\Omega \end{aligned} \tag{14}$$

If we further split virtual deformation as given in Eqs. (13)-(14), we can get

$$V_{int} = \int_\Omega \{\delta\varepsilon_{m1}\}^T \{n\} d\Omega + \int_\Omega \{\delta\varepsilon_{m2}\}^T \{n\} d\Omega + \int_\Omega \begin{Bmatrix} \{\delta\kappa\} \\ \{\delta\gamma\} \end{Bmatrix}^T \begin{Bmatrix} \{m\} \\ \{t\} \end{Bmatrix} d\Omega \tag{15}$$

Furthermore, by using Eqs. (6) and (9), we can rewrite previous equation

$$V_{int} = \int_\Omega \{\delta\varepsilon_{m1}\}^T [D_m]\{\varepsilon_{m1}\} d\Omega + \int_\Omega \begin{Bmatrix} \{\delta\kappa\} \\ \{\delta\gamma\} \end{Bmatrix}^T \begin{bmatrix} [D_\kappa] & 0 \\ 0 & [D_\gamma] \end{bmatrix} \begin{Bmatrix} \{\kappa\} \\ \{\gamma\} \end{Bmatrix} d\Omega \int_\Omega \{\delta\varepsilon_{m2}\}^T \{n\} d\Omega \tag{16}$$

Finally, we can state the weak form for the shell member that includes nonlinear strain-displacement relations

$$\begin{aligned} &\int_\Omega \begin{Bmatrix} \{\delta\varepsilon_{m1}\} \\ \{\delta\kappa\} \\ \{\delta\gamma\} \end{Bmatrix}^T \begin{bmatrix} [D_m] & 0 & 0 \\ 0 & [D_\kappa] & 0 \\ 0 & 0 & [D_\gamma] \end{bmatrix} \begin{Bmatrix} \{\varepsilon_{m1}\} \\ \{\kappa\} \\ \{\gamma\} \end{Bmatrix} d\Omega + \int_\Omega \{\delta\varepsilon_{m2}\}^T \{n\} d\Omega = \\ &= \int_\Omega \{\omega\}^T \{b\} d\Omega + \sum_{i=1}^n \int_\Omega \{\omega\}_i^T \{q\}_i d\Gamma_i + \sum_{i=1}^n \{\omega\}_i^T \{f\}_i \end{aligned} \tag{17}$$

3. Finite element formulation

Here we will define the discrete approximation based upon a flat quadrilateral shell element with four nodes. Displacements and rotations degrees of freedom are shown explicitly at the nodes as

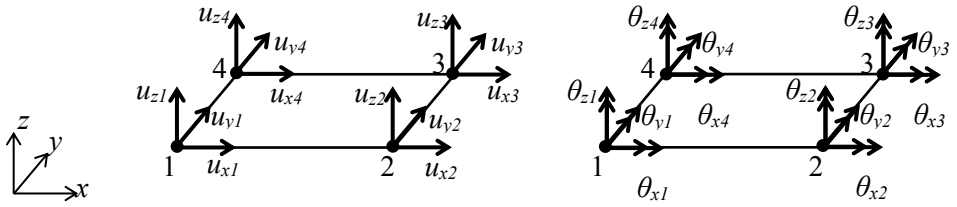

Fig. 3 Nodal displacements and rotations of shell (membrane and plate)

shown in Fig. 3.

We will first define the discrete approximation without drilling rotation θ_z, which will be included afterwards. We will use the isoparametric formulation, with shape functions defined as

$$N_1(\xi,\eta)=\frac{1}{4}(1-\xi)(1-\eta);\quad N_2(\xi,\eta)=\frac{1}{4}(1+\xi)(1-\eta)$$
$$N_3(\xi,\eta)=\tfrac{1}{4}(1+\xi)(1+\eta);\quad N_4(\xi,\eta)=\tfrac{1}{4}(1-\xi)(1+\eta) \tag{18}$$

We can write the real displacement field interpolation, by using the shape functions defined above as

$$\{u\}^{ep}=[N]\{u\}^{eh} \tag{19}$$

where vectors $\mathbf{u^e}$ and $\mathbf{u^{eh}}$ are defined as

$$\{u\}^{ep}=\{u_x^e\ \ u_y^e\ \ u_z^e\ \ \theta_y^e\ \ \theta_x^e\}^T$$
$$\{u\}^{ehT}=\{\{u\}_1^T\ \ \{u\}_2^T\ \ \{u\}_3^T\ \ \{u\}_4^T\}$$
$$\{u\}_1^T=\{u_{x1}\ \ u_{y1}\ \ u_{z1}\ \ \theta_{y1}\ \ \theta_{x1}\} \tag{20}$$

and matrix **N** is given as

$$[N]=[[N]_1\ \ [N]_2\ \ [N]_3\ \ [N]_4]$$
$$[N]_i=\begin{bmatrix}N_i & 0 & 0 & 0 & 0\\ 0 & N_i & 0 & 0 & 0\\ 0 & 0 & N_i & 0 & 0\\ 0 & 0 & 0 & N_i & 0\\ 0 & 0 & 0 & 0 & N_i\end{bmatrix} \tag{21}$$

By using previously defined results, we can write the deformation of the membrane part in matrix notation

$$\{\varepsilon_m\}=[B_m]^e\ \{u\}^e \tag{22}$$

where $\mathbf{u^e}$ is nodal displacement vector of particular shell element including rotation degree of freedom θ_z

$$\{u\}^{eT}=\{u_{x1}\ \ u_{y1}\ \ u_{z1}\ \ \theta_{y1}\ \ \theta_{x1}\ \ \theta_{z1}\cdots u_{x4}\ \ u_{y4}\ \ u_{z4}\ \ \theta_{y4}\ \ \theta_{x4}\ \ \theta_{z4}\} \tag{23}$$

In matrix $\mathbf{B_m}$ we place the corresponding derivatives of the shape functions

$$[B_m]^e=[[B_m]_1\ \ [B_m]_2\ \ [B_m]_3\ \ [B_m]_4]$$

$$[B_m]_i = \begin{bmatrix} \frac{\partial N_i}{\partial x} & 0 & & & & \\ 0 & \frac{\partial N_i}{\partial y} & 0 & 0 & 0 & 0 \\ \frac{\partial N_i}{\partial y} & \frac{\partial N_i}{\partial x} & & & & \end{bmatrix} \quad i = 1,2,3,4 \tag{24}$$

In the same manner we can also define bending deformations

$$\{\kappa\} = [B_\kappa]^e \ \{u\}^e \tag{25}$$

where $\mathbf{B}_\kappa$ is given as

$$[B_\kappa]^e = [[B_\kappa]_1 \ \ [B_\kappa]_2 \ \ [B_\kappa]_3 \ \ [B_\kappa]_4]$$
$$[B_\kappa]_i = \begin{bmatrix} 0 & 0 & 0 & \frac{\partial N_i}{\partial x} & 0 & \\ 0 & 0 & 0 & 0 & \frac{\partial N_i}{\partial y} & 0 \\ 0 & 0 & 0 & \frac{\partial N_i}{\partial y} & \frac{\partial N_i}{\partial x} & \end{bmatrix} \quad i = 1,2,3,4 \tag{26}$$

Finally, we can define shear deformations

$$\{\gamma\} = [B_\gamma]^e \ \{u\}^e \tag{27}$$

with matrix $\mathbf{B}_\gamma$ given as

$$[B_\gamma]^e = [[B_\gamma]_1 \ \ [B_\gamma]_2 \ \ [B_\gamma]_3 \ \ [B_\gamma]_4]$$
$$[B_\gamma]_i = \begin{bmatrix} 0 & 0 & \frac{\partial N_i}{\partial x} & -N_i & 0 & 0 \\ 0 & 0 & \frac{\partial N_i}{\partial y} & 0 & -N_i & 0 \end{bmatrix} \quad i = 1,2,3,4 \tag{28}$$

By combining Eqs. (24), (26) and (28), we can write the overall matrix $\mathbf{B}^e$ for a four-node flat shell element

$$[B]^e = \begin{bmatrix} [B_m]_1 \\ [B_\kappa]_1 \\ [B_\gamma]_1 \end{bmatrix} \begin{bmatrix} [B_m]_2 \\ [B_\kappa]_2 \\ [B_\gamma]_2 \end{bmatrix} \begin{bmatrix} [B_m]_3 \\ [B_\kappa]_3 \\ [B_\gamma]_3 \end{bmatrix} \begin{bmatrix} [B_m]_4 \\ [B_\kappa]_4 \\ [B_\gamma]_4 \end{bmatrix} \tag{29}$$

Thus we can compute the work of internal forces, given in Eq (17), as the sum of the corresponding element-wise computations

$$\sum_{n=1}^{nel} \int_\Omega \{\omega\}^T \ \ [B^e]^T \ \ [D^e][B^e]\{u\} d\Omega$$
$$= \{\omega\}^T \sum_{n=1}^{nel} \int_\Omega [B^e]^T \ \ [D^e] \ [B^e] d\Omega \{u\} \tag{30}$$

From the last result, we can define the material part of the stiffness matrix:

$$[K^e] = \int_{A^e} [B^e]^T [D^e][B^e] dA^e$$
$$= \int_{-1}^{1} \int_{-1}^{1} [B^e]^T [D^e][B^e] \det[J] \, d\xi d\eta \tag{31}$$

where **J** is Jacobian matrix given by

$$[J]=\begin{bmatrix}\frac{\partial x}{\partial \xi} & \frac{\partial y}{\partial \xi}\\ \frac{\partial x}{\partial \eta} & \frac{\partial y}{\partial \eta}\end{bmatrix} \tag{31}$$

By rewriting the second part of virtual membrane deformations, given in Eqs. (12)-(13) in matrix notation

$$\{\delta\varepsilon_{m2}\}=\begin{bmatrix}\frac{\partial w_z}{\partial x} & 0\\ 0 & \frac{\partial w_z}{\partial y}\\ \frac{\partial w_z}{\partial y} & \frac{\partial w_z}{\partial x}\end{bmatrix}\begin{Bmatrix}\frac{\partial u_z}{\partial x}\\ \frac{\partial u_z}{\partial y}\end{Bmatrix} \tag{32}$$

we can also define the geometric part of the stiffness matrix form the second integral in Eq. (17)

$$\int_A \{\delta\varepsilon_{m2}\}^T \ \{n\}dA=\int_A \begin{Bmatrix}\frac{\partial \omega_z}{\partial x} & \frac{\partial \omega_z}{\partial y}\end{Bmatrix}\begin{bmatrix}n_x & n_{xy}\\ n_{xy} & n_y\end{bmatrix}\begin{Bmatrix}\frac{\partial u_z}{\partial x}\\ \frac{\partial u_z}{\partial y}\end{Bmatrix}dA \tag{33}$$

where explicit form of the matrices given in Eq. (33) can be written as

$$\begin{gathered}\{\varepsilon_3\}=[B_3]\{u^e\}\\ \{\delta\varepsilon_3\}^T=\{\omega^e\}^T[B_3]^T\end{gathered} \tag{34}$$

whereas matrix $\mathbf{B_3}$ is given by

$$\begin{gathered}[B_3]^e=[[B_3]_1\ [B_3]_2\ [B_3]_3\ [B_3]_4]\\ [B_3]_i=\begin{bmatrix}0 & 0 & \frac{\partial N_i}{\partial x} & 0 & 0 & 0\\ 0 & 0 & \frac{\partial N_i}{\partial y} & 0 & 0 & 0\end{bmatrix}\quad i=1,2,3,4\end{gathered} \tag{35}$$

We note that the result in Eq. (33) can also be computed as a sum by all elements

$$\sum_{e=1}^{nel}\int_A \{\delta\varepsilon_3\}^T\ [n]\{\varepsilon_3\}^T dA=\{\omega^e\}^T\ \sum_{e=1}^{nel}\int_A\ [B_3^e]^T\ [n][B_3^e]dA\{u^e\} \tag{36}$$

Finally we can write the compact form of the geometric part of the stiffness matrix

$$\left[K_g\right]=\int_{-1}^{1}\int_{-1}^{1}[B_3^e]^T\ [n][B_3^e]\det[J]\,d\xi d\eta \tag{37}$$

3.1 Including drilling rotation

Since our goal is to combine shell elements with space beam elements, we should also include a rotation about *z* axis, or so-called drilling rotation (Allman 1984). A detailed formulation can be found in (Ibrahimbegovic *et al*. 1990b), with only a brief presentation given herein.

By taking into account the drilling rotation, the displacement field can be defined as

$$u_x(\xi,\eta)=\sum_{a=1}^{4}N_a\cdot u_{xa}^e+\sum_{k=5}^{8}\frac{\Delta y_{ab}}{8}N_k^*\cdot(\theta_{zb}-\theta_{za});\quad \theta_y(\xi,\eta)=\sum_{a=1}^{4}N_a\cdot\theta_{ya}^e$$

$$u_y(\xi,\eta)=\sum_{a=1}^{4}N_a\cdot u_{ya}^e-\sum_{k=5}^{8}\frac{\Delta x_{ab}}{8}N_k^*\cdot(\theta_{zb}-\theta_{za});\quad \theta_x(\xi,\eta)=\sum_{a=1}^{4}N_a\cdot\theta_{xa}^e$$
$$u_z(\xi,\eta)=\sum_{a=1}^{4}N_a\cdot u_{za}^e \tag{38}$$

where

$$\begin{matrix}\Delta y_{ab}=y_b-y_a\\ \Delta x_{ab}=x_b-x_a\end{matrix}\qquad b=\begin{cases}a+1;\ a=1,2,3\\ 1;\qquad a=4\end{cases} \tag{39}$$

whereas N_k^* are the Serendipity shape functions, formulated for the mid-side nodes of the 8-node element (Ibrahimbegovic and Wilson 1991):

$$N_5^*(\xi,\eta)=\frac{1}{2}(1-\xi^2)(1-\eta);\qquad N_6^*(\xi,\eta)=\frac{1}{2}(1+\xi)(1-\eta^2)$$
$$N_7^*(\xi,\eta)=\frac{1}{2}(1-\xi^2)(1+\eta);\qquad N_8^*(\xi,\eta)=\frac{1}{2}(1-\xi)(1-\eta^2) \tag{40}$$

In Eq. (39) indices *a*, *b* and *k* can take the values defined by following combinations: (1, 2, 5), (2, 3, 6), (3, 4, 7), (4, 1, 8).

The corresponding deformation takes the value

$$\{\varepsilon_m\}=symm\nabla\{u_m\}=\sum_{i=1}^{4}[B_m^*]_i\,\{u_m^*\}_i \tag{41}$$

The displacement vector from Eq. (41) is defined as

$$\{u_m^*\}_i=\{u_{xi}\quad u_{yi}\quad \theta_{zi}\}^T \tag{42}$$

and strain-displacement matrix is defined by the shape functions' derivatives

$$[B_m^*]_i=\begin{bmatrix}\frac{\partial N_i}{\partial x} & 0 & \frac{\partial N_{xi}}{\partial x}\\ 0 & \frac{\partial N_i}{\partial y} & \frac{\partial N_{Yi}}{\partial y}\\ \frac{\partial N_i}{\partial y} & \frac{\partial N_i}{\partial x} & \frac{\partial N_{xi}}{\partial y}+\frac{\partial N_{Yi}}{\partial x}\end{bmatrix} \tag{43}$$

where N_X and N_Y are Allman's incompatible shape functions

$$N_{Xi}=\frac{1}{8}\left(\Delta y_{ij}N_l-\Delta y_{ik}N_m\right)$$
$$N_{Yi}=\frac{1}{8}\left(\Delta x_{ij}N_l-\Delta x_{ik}N_m\right) \tag{44}$$

Indices *i*, *j*, *k*, *l* and *m* in Eq. (44) can be defined in FORTRAN-like manner as

$$i=1,2,3,4;\qquad m=i+4;\qquad l=m-1+4int\left(\frac{1}{i}\right);$$
$$k=mod(m,4)+1;\qquad j=l-4 \tag{45}$$

The skew-symmetric deformation can be written as

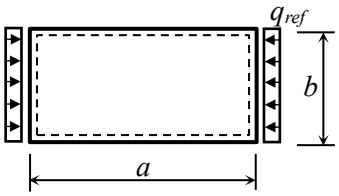

Fig. 4 Example plate layout

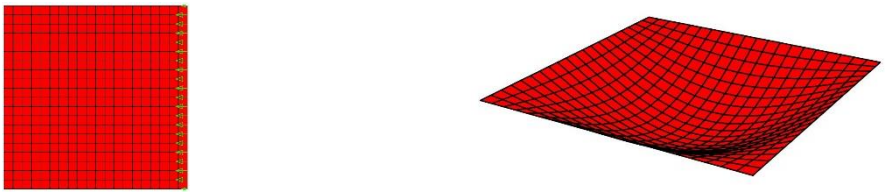

(a) Square plate with applied load (b) First buckling mode

Fig. 5 Plate with span ratio *a*/*b*=1

$$\{\varepsilon_{sk}\} = skew\nabla\{u_m\} = \sum_{i=1}^{4}[b]_i\{u_m^*\}_i + \theta_z \tag{46}$$

where matrix **b** is defined as

$$\{b\}_i = \begin{pmatrix} -\frac{1}{2}\frac{\partial N_i}{\partial y} \\ \frac{1}{2}\frac{\partial N_i}{\partial y} \\ \frac{1}{16}\left(-\Delta y_{ij}\frac{\partial N_l}{\partial y} + \Delta y_{ik}\frac{\partial N_m}{\partial y} + \Delta x_{ij}\frac{\partial N_l}{\partial x} + \Delta x_{ik}\frac{\partial N_m}{\partial x}\right) - N_i \end{pmatrix} \tag{47}$$

Gathering these results we finally arrive at the stiffness matrix form for membrane part, which can be written as

$$[K_m] = [K_m^*] + [P_\gamma] = \int_\Omega [B_m^*]^T\ [D_m][B_m^*]d\Omega + \gamma\int_\Omega \{b\}^T\ \{b\}d\Omega \tag{48}$$

4. Numerical examples

In this section we consider several numerical examples in order to illustrate performance of this element in application to buckling problems. All numerical computations were performed by a research version of the computer code FEAP (see Zienkiewicz and Taylor 2005).

4.1 Validation examples

4.1.1 Rectangular plate in-plane buckling

We have already stated (see Eq. (2)) that the analytical solution for the critical compression load of a rectangular plate depends on span ratio (*a*/*b*). Here we check this result with validation computations of the plate critical load for two different values of *a*/*b* ratio. One analysis is carried out for *a*=*b*=500 mm (Fig. 5), resulting with span ratio 1, and another for span ratio *a*/*b*=2, with

(a) Rectangular plate with applied load (b) First buckling mode

Fig. 6 Plate with span ratio $a/b = 2$

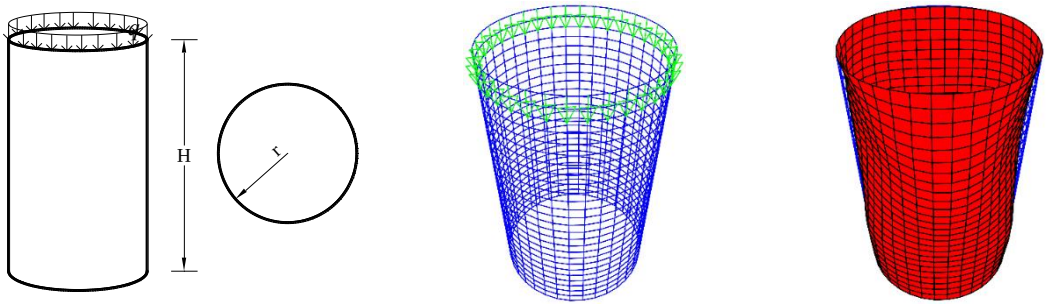

(a) Cylinder geometry (b) Finite element model (c) First buckling mode

Fig. 7 Buckling analysis of cylinder

a=1000 mm and b=500 mm (Fig. 6). The thickness of the plate in both cases is t=5.0 mm, Young modulus $2 \cdot 10^5$ *MPa* and Poisson's ratio 0.3. The plate is simply supported at all four edges, and it is subjected to in plane compression (see Fig. 4).

By taking into account the chosen values of span ratio, we can compute the minimum value of buckling coefficient k_σ given in Eq. (2). For both span ratios we obtained k_σ=4.0. Further, by using the Eq. (2) the critical load value for the considered plates is q_{cr}=361.5 N/mm.

The same examples were computed using the proposed finite element model for linear buckling analysis. We use mesh of 20×20 4-node quadrilateral shell elements for each case.

By using the model in Fig. 5(a), we obtain the critical load q_{cr}=362.4 N/mm, which is an increase of 0.25 % compared to the critical load value obtained by analytical solution. The first buckling mode of the plate is in Fig. 5(b). Next, we analyse buckling load of the rectangular plate with span ratio a/b=2 (Fig. 6).

The first buckling mode for the rectangular plate is pictured in Fig. 6(b). The computed critical load is q_{cr}=362.6 N/mm, which when compared against analytical solution, represent an increase of 0.30 %. We can conclude that presented examples give us a good match of the analytical results and results obtained using the finite element model.

4.1.2 Cylinder buckling

In order to show that the proposed model can provide good results for critical load also in the case with more complex geometry, we will further compute the critical load of a cylinder (Fig. 7).

The chosen height of the cylinder is H=260.0 mm, its radius r=80.0 mm and its thickness t=3.0 mm. We also choose: Young's modulus $E=10^7$ N/cm^2 and Poisson ratio v=0.3. The pressure load is applied as indicated in Fig. 7(a)-(b). The mesh of finite elements consists of 26 elements per cylinder height and 36 elements per perimeter of the base circle. Since we use flat shell elements, we need to choose more elements to represent the geometry of the cylinder more accurate. The nodes at the

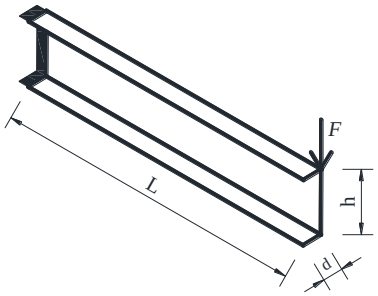

L = 36.0 cm
D = 2.0 cm
H = 6.0 cm
t = 0.05 cm
E = 10^7 N/cm^2
v = 0.333

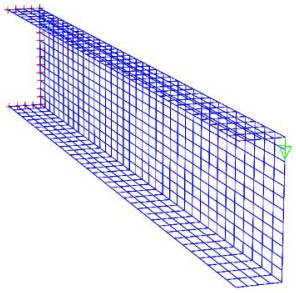

(a) Cantilever geometry (c) Finite element model

Fig. 8 Buckling analysis of U-shaped cantilever

bottom of the cylinder have all the displacements restrained. The first buckling mode is given in Fig. 7(c). Proposed approach for linear buckling analysis gives the critical load value q_{cr}=6.88·10^3 N/mm.

We can compare this value against the analytical solution for the cylinder with compression load applied on its top, which can be found in a reference books (e.g., Timoshenko and Gere 1962)

$$q_{cr} = \frac{Et^2}{r\sqrt{3(1-v^2)}} \tag{49}$$

For the cylinder in Fig. 7, analytical solution gives us critical load value q_{cr}=6.81·10^3 N/mm. The critical load obtained by using finite element linear buckling analysis results in an increase of 1% when compared against the analytical solution. We can conclude that the finite element model gives very good results.

4.2 Stability of U-shaped cantilever beam

In following example we analyse stability of the U-shaped cantilever beam (Fig. 8). We take all geometric and material properties of the beam from (Ibrahimbegovic and Fray 1994a), where the cantilever was computed by using finite deformation shell elements. By using 4-node geometrically nonlinear shell element, authors computed value of the critical force F_{cr}=140 N.

First, we use the same finite element mesh of 12×10 elements that the authors used in the reference paper. The computed vale of the critical force is F_{cr}=183.92 N, which is an increase of 30% compared to the result obtained by using nonlinear analysis in (Ibrahimbegovic and Fray 1994a). The buckling modes are shown in Fig. 9. Next, we use mesh of 36×20 elements (Fig. 8(c)), and computed critical force for this case is F_{cr}=172.4 N, which when compared against nonlinear computation represents an increase of 23%. Further mesh refinement does not significantly change the results.

The difference in the obtained results of nonlinear versus linear instability computation, where the nonlinear model can take into account large pre-buckling displacements, which can significantly reduce the buckling load. This example clearly illustrates the need to add the stiffeners in order to prevent large values of pre-buckling displacements.

4.3 Stability of steel plate girders

In this example we analyze stability of a steel plate girder. The girder cross-section is welded I-

(a) First buckling mode (b) Second buckling mode

Fig. 9 Buckling modes of U-shaped cantilever beam

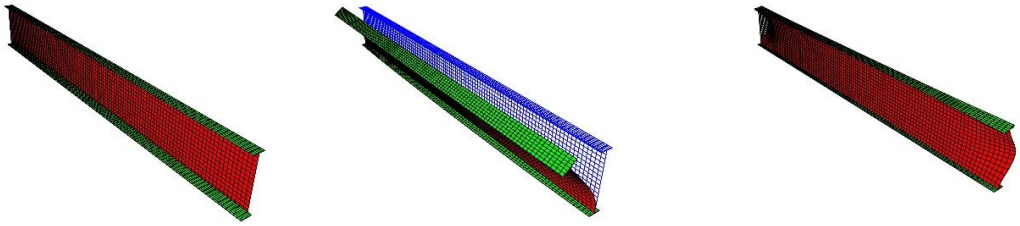

(a) Girder FE mesh (b) Lateral torsional buckling (c) Web buckling of laterally braced girder

Fig. 10 Stability of a steel plate girder

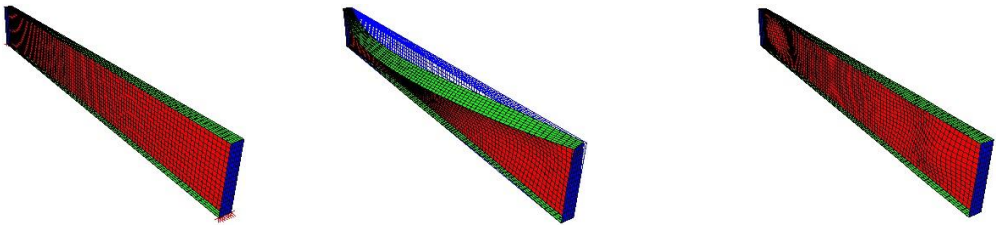

(a) Girder FE mesh (b) Lateral torsional buckling (c) Web buckling of laterally braced girder

Fig. 11 Stability of a steel plate girder with end stiffeners

shaped section. Geometric properties of the flange are: width b_f=300.0 mm, thickness t_f=20.0 mm. The chosen web geometric properties are: height h_w=1500.0 mm, thickness t_w=8.0 mm. Web transverse stiffeners thickness is t_s=12.0 mm. Girder span is 11.20 m. Stiffeners are placed at every 1.40 m, and at the ends of the beam at 0.70 m. The elastic modulus is $2.1 \cdot 10^8$ kN/m^2, and Poisson's ratio 0.30. Quadrilateral 4-node shell elements are used for modelling the girder. The girder is hinged at both ends. Distributed load q=10.0 kN/m is applied to the upper flange in the plane of the web.

First, we give results for the case when girder has no stiffeners and it is not laterally braced (Fig. 10(a)-(b)). Lateral torsional buckling occurs (Fig. 10(b)), and the critical load parameter obtained by this computation is 3.85607907E-01, which gives the critical load value q_{cr}=3.86 kN/m.

Next we put three lateral braces at the upper flange level. The braces are placed at both ends and in the middle of the beam span. Since lateral torsional buckling is prevented, it is the girder web that buckles (Fig. 10(c)). New computed critical load parameter is 2.87857360E+00, and the critical load value q_{cr}=28.78 kN/m. By preventing lateral displacements in just three points, increases value of critical load by 7.5 times.

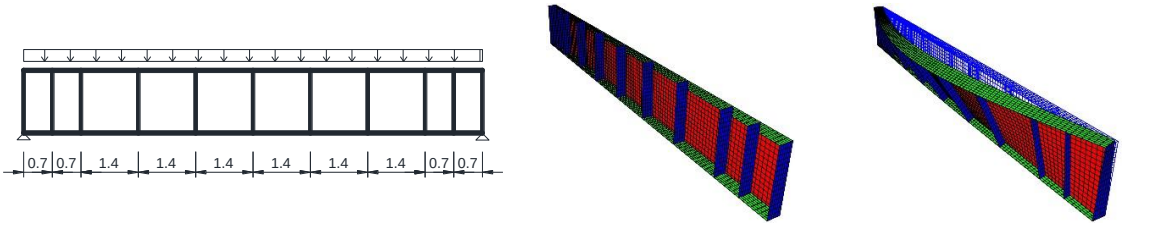

(a) Transverse stiffeners spacing (b) Girder model (c) Lateral torsional buckling mode (no lateral braces)

Fig. 12 Stability of a steel plate girder with stiffeners

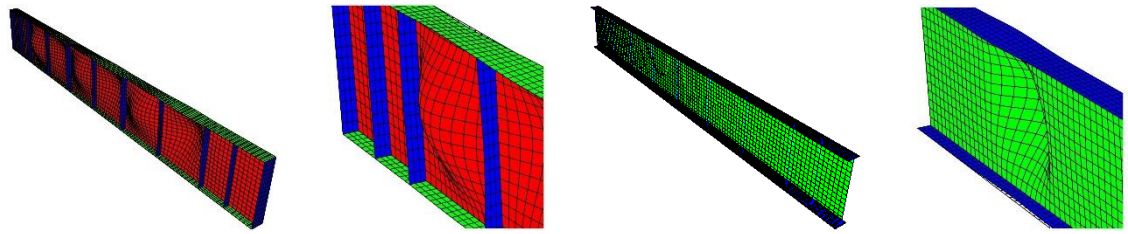

(a) Buckling of the web (b) First buckling mode (c) Girder with frame stiffeners (d) Buckling of web with frame stiffeners

Fig. 13 Stability of a steel plate girder with stiffeners and lateral bracings

Since the welded I-shaped sections are very flexible, especially their web, generally they are designed with stiffeners. Number of web stiffeners can differ, but they are placed at least at both ends of the girder. Next, we give results of buckling analysis of such a girder with two stiffeners (Fig. 11). Note that nodes of the stiffeners at lower flange are hinged. In this case stiffeners support not only the web, but also the upper flange, which effects overall stiffness of the girder. The stiffeners prevent lateral movement of upper flange ends, which results in an increase in value of the critical load q_{cr}=51.81 kN/m. The first buckling mode is in Fig. 11(b).

Furthermore, we prevent lateral displacement of the upper flange by imposing additional restraints along the flange. Since the stiffeners support both ends of the web the computed critical load is q_{cr}=71.13 kN/m (Fig. 11(c)).

Next we analyse girder with transverse stiffeners and without lateral braces (Fig. 12(a)-(b)). Again, lateral torsional buckling occurs (Fig. 12(c)), and the critical load value is q_{cr}=61.84 kN/m.

In Fig. 13 are given computed results for braced girder with stiffeners. In case with only three lateral braces and stiffeners modelled as shell elements, the critical load is q_{cr}=101.22 kN/m. If we put braces along the length of upper flange, which is common case in engineering practice, critical load value is q_{cr}=101.47 kN/m. The last two results do not differ much because it is the web of the girder that buckles in both cases. Next, transverse stiffeners are modelled by using space frame elements (Ibrahimbegovic *et al*. 2013.) capable to take into account linear buckling, Fig. 13(c)-(d). The value we obtain for the critical load is q_{cr}=105.09 kN/m. By comparing results for the case when stiffeners are modelled as shell elements against the case when they are modelled as frame elements, the percentage difference between the two results is 3.5 %. This indicates that it is quite possible to use the frame element for modelling stiffeners in further computations.

By varying the spacing of stiffeners, we obtain results given in Fig. 14(a) for distributed load q and in Fig. 14(b) for point load F, which is applied in the middle of the girder span.

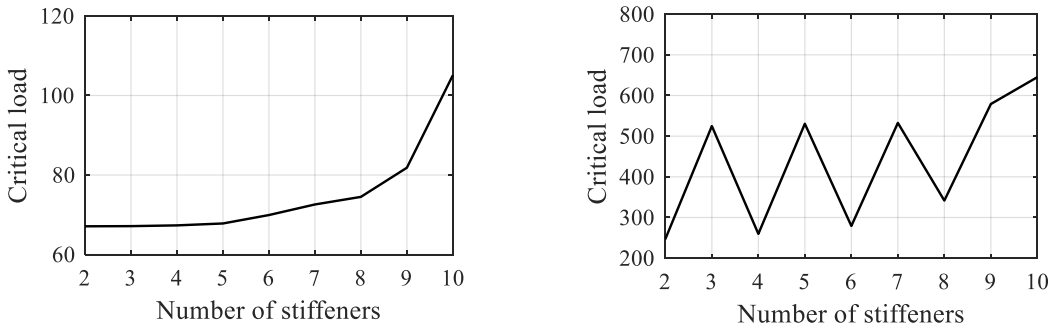

(a) Girder loaded with distributed load (b) Girder loaded with point load

Fig. 14 Critical load – stiffeners spacing curve

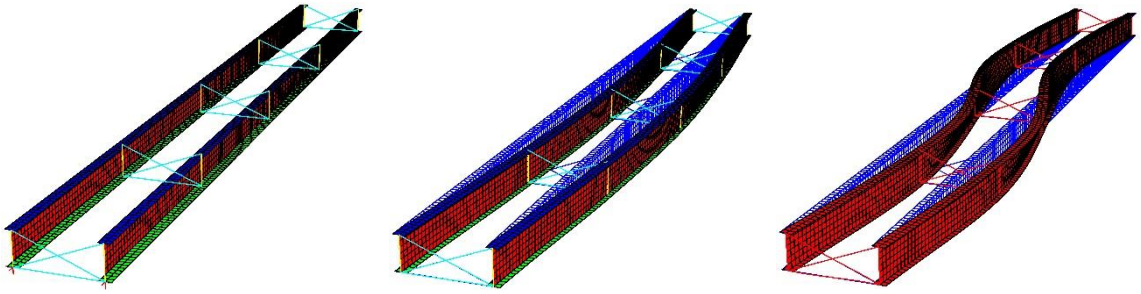

(a) Girder FE mesh (b) First buckling mode (c) Second buckling mode

Fig. 15 Stability of a steel plate girder bridge during the construction

Peaks on the graph in Fig. 14(b) are values of critical force F when there is a transverse stiffener in the middle of the span of the web, under the applied point load. As it can be seen, lower value of F_{cr} is obtained when point load is placed in the middle of stiffener spacing. During each analysis, the stiffeners are set at constant spacing. Only in case of ten stiffeners, the spacing of stiffeners at both ends of girder is twice shorter (Fig. 14(a)-(b)).

4.4 Stability of plate girder bridge

A plate girder bridge is a typical case of the use of welded steel plate sections. Here, we will perform buckling analysis of such a bridge. The bridge bearing structure consists of two parallel plate girders that are connected by bar connectors along the span. We analyse two possible cases. The first case is stability of the girder during construction, when a concrete deck is not set over the girders. In those circumstances, lateral torsional buckling of girders is possible to occur due to load caused by concrete slab construction. The second analysis is performed for girders in exploitation phase when concrete slab is hardened, and now the web of the girder can buckle. Both types of analysis are performed for gravity imposed distributed load, applied on the upper flange of both girders.

Chosen geometric and material properties of the structure are partially taken from Hendy and Murphy 2007. More precisely, we take one span of those authors' continuous beam, and we compute it as a simply supported beam. The distance between web stiffeners is also changed, and we study

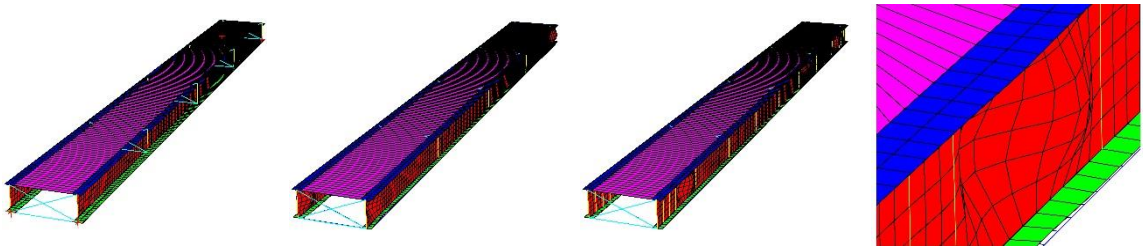

(a) Girder FE mesh (b) First buckling mode (c) First buckling mode (more stiffeners) (d) Detail of web buckling

Fig. 16 Stability of a steel plate girder with stiffeners and lateral bracings

Table 1 Values of the critical load for the plate girder bridge

Phase	Construction phase		Exploitation phase	
Stiffeners spacing	8.0 m	4.0 m	4.0 m	4.0 m and 1.2 m
Critical load	28.725 kN/m	30.160 kN/m	306.30 kN/m	659.50 kN/m

two cases when the distance is 8.0 m and 4.0 m. The flange width is b_f=0.40 m, thickness of the lower flange is t_{fd}=0.04 m, while thickness of the upper flange is t_{fg}=0.025 m, the web height is h_w=1.20 m, and thickness of the web is t_w=0.025 m. The span of the girder is 32.00 m. Transverse stiffeners of the web have thickness of t_p=0.02 m, and their width is b_p=0.10 m. Two parallel girders are connected using L shaped steel bars 150×150×18. Flanges of the girders are modelled using shell elements, as well as webs and concrete slab. Stiffeners and *L* bars are modelled using frame elements.

Computed results for steel girders during construction phase are given in Fig. 15. The first and the second buckling modes can be seen in Fig. 15(b)-(c). These results are for the case when spacing between stiffeners is 8.0 m. In Fig. 16 we show results for the exploitation phase, when concrete slab is added to the model. First buckling mode, for the case when stiffeners are placed at every 8.0 m, is given in Fig. 16(b). In Fig. 16(c)-(d) we show the first buckling mode for the case when spacing of stiffeners is 4.0 m, while in the area closer to the both ends, spacing of stiffeners is 1.2 m.

The critical load values for all different cases described above are given in Table 1. The obtained results show that the plate girders are sensitive to lateral torsional buckling during the construction. For the case when the concrete slab is included, the critical load is about 10 times greater than the one obtained in the construction phase. This is an important issue that needs to be taken into account throughout the design process. The analysis presented herein shows that the proposed model can be extremely helpful. Engineers in everyday practice take precautions during the construction phase of the bridge in order to avoid this kind of buckling failure.

5. Conclusions

In this paper we deal with buckling of steel plate girders by using shell elements. The proposed finite element procedure is capable to analyze buckling problems for very complex structures, yet it remains a simple tool for computing the critical load by solving general eigenvalue problem.

The numerical examples have shown how critical load is changing in function of stiffeners

location. Similar analysis can be performed varying other geometrical characteristics, web or stiffeners thickness for example. Performing these kind of tests can help engineers to optimize geometry of the girder, thickness of plates, spacing of lateral bracings and other design parameters. We also show useful combination of shell and frame elements, and possibility to replace some shell elements with 3d frame elements that include linear buckling procedure, without much affecting the results accuracy.

Acknowledgments

This work was supported by scholarship of French Embassy in Sarajevo. AI was also supported by IUF-Institut Universitaire de France. This support is gratefully acknowledged.

References

Allman, D. (1984), "Compatible triangular element including vertex rotations for plane elasticity analysis", *Comput. Struct.*, **19**, 1-8. https://doi.org/10.1016/0045-7949(84)90197-4.

Bas, S. (2019), "Lateral torsional buckling of steel I-beams: Effect of initial geometric imperfection", *Steel Compos. Struct.*, **30**, 483-492. https://doi.org/10.12989/scs.2019.30.5.483.

Bathe, K.J. (1996), *Finite Element Procedures*, Prentice-Hall, Englewood Cliffs, New Jersey, USA.

Bradford, M.A. and Liu, X. (2016), "Flexural-torsional buckling of high-strength steel beams", *J. Constr. Steel Res.*, **124**, 122-131. https://doi.org/10.1016/j.jcsr.2016.05.009.

Chajes, A. (1974), *Principles of Structural Stability*, Prentice Hall College Div., New Jersey, USA.

Ellobodya, E. (2017), "Interaction of buckling modes in railway plate girder steel bridges", *Thin Wall. Struct.*, **115**, 58-75. https://doi.org/10.1016/j.tws.2016.12.007.

Eurocode 3 (2006), Design of Steel Structure s-Part 1-5: Plated Structural Elements, EN 1993-1-5:2006 E, CEN-European Comitee for Standardization.

Gonçalves, R. (2019), "An assessment of the lateral-torsional buckling and post-buckling behaviour of steel I-section beams using a geometrically exact beam finite element", *Thin Wall. Struct.*, **143**, 106-222. https://doi.org/10.1016/j.tws.2019.106222.

Hendy, C. and Murphy, C. (2007), *Designers' Guide to EN 1993-2*, Steel Bridges, Thomas Telford, UK.

Ibrahimbegovic, A. and Frey, F. (1995), "Variational principles and membrane finite elements with drilling rotations for geometrically non-linear elasticity", *Int. J. Numer. Meth. Eng.*, **38**, 1885-1900. https://doi.org/10.1002/nme.1620381106.

Ibrahimbegovic, A. (1994), "Stress resultant geometrically nonlinear shell theory with drilling rotations. Part I: A consistent formulation", *Comput. Meth. Appl. Mech. Eng.*, **118**, 265-284. https://doi.org/10.1016/0045-7825(94)90003-5.

Ibrahimbegovic, A. (1995), "On finite element implementation of geometrically nonlinear Reissner's beam theory: three-dimensional curved beam elements", *Comput. Meth. Appl. Mech. Eng.*, **122**, 11-26. https://doi.org/10.1016/0045-7825(95)00724-F.

Ibrahimbegovic, A. (2009), *Nonlinear Solid Mechanics: Theoretical Formulations and Finite Element Solution Methods*, Springer, Berlin, Germany.

Ibrahimbegovic, A. and Fray, F. (1993), "Finite element analysis of linear and non-linear planar deformations of elastic initially curved beams", *Int. J. Numer. Meth. Eng.*, **36**, 3239-3258. https://doi.org/10.1002/nme.1620361903.

Ibrahimbegovic, A. and Frey, F. (1994a), "Stress resultant geometrically nonlinear shell theory with drilling rotations-Part II. Computational aspects", *Comput. Meth. Appl. Mech. Eng.*, **118**, 285-308. https://doi.org/10.1016/0045-7825(94)90004-3.

Ibrahimbegovic, A. and Frey, F. (1994b), "Stress resultant geometrically nonlinear shell theory with drilling rotations. Part III: Linearized kinematics", *Int. J. Numer. Meth. Eng.*, **37**, 3659-3683. https://doi.org/10.1016/0045-7825(94)90004-3.

Ibrahimbegovic, A. and Wilson, E. L. (1991), "A unified formulation for triangular and quadrilateral flat shell finite elements with six nodal degrees of freedom", *Commun. Appl. Numer. Meth.*, **7**, 1-9. https://doi.org/10.1002/cnm.1630070102.

Ibrahimbegovic, A. and Wilson, E.L. (1990), "Automated truncation of Ritz vector basis in modal transformation", *ASCE J. Eng. Mech. Div.*, **116**, 2506-2520. https://doi.org/10.1061/(ASCE)0733-9399(1990)116:11(2506).

Ibrahimbegovic, A., Chen, H.C., Wilson, E.L. and Taylor, R.L. (1990a), "Ritz method for dynamic analysis of linear systems with non-proportional damping", *Int. J. Earthq. Eng. Struct. Dyn.*, **19**, 877-889. https://doi.org/10.1002/eqe.4290190608.

Ibrahimbegovic, A., Hajdo, E. and Dolarevic, S. (2013), "Linear instability or buckling problems for mechanical and coupled thermomechanical extreme conditions", *Coupl. Syst. Mech.*, **2**, 349-374. https://doi.org/10.12989/csm.2013.2.4.349.

Ibrahimbegovic, A., Shakourzadeh, H., Batoz, J.L., Al Mikdad, M. and Guo, Y.Q. (1996), "On the role of the geometrically exact and second-order theories in buckling and post-buckling analysis of three-dimensional beam structure", *Comput. Struct.*, **61**, 1101-1114. https://doi.org/10.1016/0045-7949(96)00181-2.

Ibrahimbegovic, A., Taylor, R.L. and Wilson, E.L. (1990), "A robust membrane quadrilateral element with drilling degrees of freedom", *Int. J. Numer. Meth. Eng.*, **30**, 445-457. https://doi.org/10.1002/nme.1620300305.

Imamovic, I., Ibrahimbegovic, A. and Mesic, E. (2017), "Nonlinear kinematics Reissner's beam with combined hardening/softening elastoplasticity", *Comput. Struct.*, **189**, 12-20. https://doi.org/10.1016/j.compstruc.2017.04.011.

Imamovic, I., Ibrahimbegovic, A. and Mesic, E. (2018), "Coupled testing-modeling approach to ultimate state computation of steel structure with connections for statics and dynamics", *Coupl. Syst. Mech.*, **7**, 555-581. https://doi.org/10.12989/csm.2018.7.5.555.

Kala, Z. (2015), "Sensitivity and reliability analyses of lateral-torsional buckling resistance of steel beams", *Arch. Civil Mech. Eng.*, **15**, 1098-1107. https://doi.org/10.1016/j.acme.2015.03.007.

Kala, Z. and Valeš, J. (2017), "Global sensitivity analysis of lateral-torsional buckling resistance based on finite element simulations", *Eng. Struct.*, **134**, 37-47. https://doi.org/10.1016/j.engstruct.2016.12.032.

Ngo, V.M., Ibrahimbegovic, A. and Hajdo, E. (2014), "Nonlinear instability problems including localized plastic failure and large deformations for extreme thermo-mechanical conditions", *Coupl. Syst. Mech.*, **3**, 89-110. https://doi.org/10.12989/csm.2014.3.1.089.

Ozbasaran, H. and Yilmaz, T. (2018), "Shape optimization of tapered I-beams with lateral-torsional buckling, deflection and stress constraints", *J. Constr. Steel Res.*, **143**, 119-130. https://doi.org/10.1016/j.jcsr.2017.12.022.

Sahraei, A. and Mohareb, M. (2019), "Lateral torsional buckling analysis of moment resisting plane frames", *Thin Wall. Struct.*, **134**, 233-254. https://doi.org/10.1016/j.tws.2018.10.006.

Saliba, N. and Gardner, L. (2013), "Experimental study of the shear response of lean duplex stainless steel plate girders", *Eng. Struct.*, **46**, 375-391. https://doi.org/10.1016/j.engstruct.2012.07.029.

Serror, M.H., Hamed, A.N. and Mourad, S.A. (2016), "Numerical study on buckling of steel web plates with openings", *Steel Compos. Struct.*, **22**, 1417-1443. https://doi.org/10.12989/scs.2016.22.6.1417.

Timoshenko, S. and Gere, J. (1962), *Theory of Elastic Stability*, McGraw-Hill, New York, NY, USA.

Timoshenko, S. and Woinowsky-Krieger, S. (1959), *Theory of Plates and Shells*, McGraw-Hill, New York, NY, USA.

Ventsel, E. and Krauthammer, T. (2001), *Thin Plates and Shells*, Marcel Dekker, New York, USA.

Zienkiewicz, O.C. and Taylor, R.L. (2005), *The Finite Element Method*, Vols. I, II, III, Elsevier, Oxford, UK.